Performance-Based Assessment and Design of Structures on Liquefiable Soils: from Triggering to Consequence and Mitigation

Shideh Dashti1[1], Zachary Bullock[2], and Yu-Wei Hwang[3]

[1] University of Colorado Boulder, Boulder, CO USA
[2] University of British Columbia, Vancouver, BC Canada
[3] University of Texas at Austin, Austin, TX USA

Abstract. Effective liquefaction mitigation requires an improved fundamental understanding of triggering in terms of excess pore pressures in realistically stratified deposits that experience cross-layer interactions as well as performance-based consequence procedures that account for 3D soil-structure interaction (SSI), all mechanisms of deformation, total uncertainty, and the impact of mitigation. In this paper, we first present a series of centrifuge experiments to evaluate site response and pore pressure generation in layered liquefiable deposits, soil-structure interaction (SSI), and the impact of ground densification as a mitigation strategy on SSI and building performance. Second, experimental results are used to validate 1D and 3D, fully-coupled, nonlinear, dynamic finite element analyses of layered sites and soil-foundation-structure systems with and without mitigation. Third, numerical parametric studies (exceeding 167,000 1D and 63,000 3D simulations) are used to identify the functional forms for predicting liquefaction triggering in the free-field based on the capacity cumulative absolute velocity (CAV_c) required to achieve a threshold excess pore pressure ratio (r_u), settlement of unmitigated structures, and the relative impact of ground densification on foundation's permanent settlement. And finally, a limited case history database is used validate the triggering and consequence models, accounting for field complexities not captured numerically or experimentally. This integrative approach yields a set of procedures that are the first to consider variations in soil layering and geometry, layer-to-layer cross interactions, foundation and structure properties (in 3D), contribution of all mechanisms of deformation below unmitigated structures, geometry and properties of densification, ground motion's cumulative characteristics, total inherent model uncertainties, and the explicit conditionality of structural settlement on free-field triggering—which are necessary to realize the benefits of performance-based engineering in liquefaction assessment.

Keywords: Liquefaction triggering, mitigation, soil-structure interaction.

1 Introduction and Background

Probabilistic predictive models for the triggering (e.g., Seed et al. 2003; Boulanger and Idriss 2012; Maurer et al. 2017) and consequences (e.g., Bray and Macedo 2017; Bullock et al. 2019a,b) of soil liquefaction are becoming increasingly common in the design of structures founded on such deposits. However, the application of triggering and consequence procedures remains primarily disconnected, because their methodological approaches and implementation remain separate. The most recent probabilistic consequence models (e.g., Bullock et al. 2019a,b), which are capable of predicting the settlement and tilt of isolated shallow-founded structures on layered soil systems with evolutionary ground motion intensity measures (IMs), do not explicitly depend on evaluation of triggering (e.g., in terms of FS_{liq}). However, through inclusion of case histories in their formulation, these models remain implicitly conditioned on the occurrence of liquefaction or its surface manifestation. This implicit conditioning has the potential to lead to overestimation of the risk of liquefaction consequences.

The existing models for predicting the occurrence of liquefaction have their own set of limitations. They are often based on empirical observations of surface manifestation of liquefaction (e.g., Cetin and Seed 2004; Idriss and Boulanger 2008) or mechanistic prediction of $r_u = 1$; where $r_u = \Delta u/\sigma'_{vo}$. Meanwhile, it is known that partial or full liquefaction may occur without necessarily generating surface manifestations in the form of sand boils or ejecta. These procedures typically focus on individual soil layers and do not consider layer cross interactions (Beyzaei et al. 2018), which can influence the manifestation and propagation of damage. The procedures typically rely on the cyclic stress ratio (CSR) at the surface to define the demand by interpolating PGA at non-liquefied free-field sites, which is not necessarily an optimum choice of IM and ignores the degree of softening and pore pressure generation in soil. Lastly, the mechanistic procedures do not acknowledge that significant softening and deformations can still occur at r_u values less than 1.0.

After evaluating the likelihood of triggering and consequence, an engineer often needs to consider different forms of ground improvement and mitigation. None of the existing procedures for ground improvement consider the presence and/or interaction of a structure with soil, the active mechanisms of deformation near a structure, or the underlying uncertainties. In designing ground densification for instance, engineers commonly rely on empirical triggering or volumetric settlement estimations in the free-field, or at best semi-empirical probabilistic consequence models that do not consider densification dimensions in relation to and in interaction with the overlying structure. Additionally, since mitigation is often designed based on free-field triggering calculations (i.e., FS_{liq} in various soil layers), the evaluation of post-mitigation triggering and consequence may also be implicitly conditioned on the occurrence of liquefaction in free-field conditions. This conditioning exists because the size of the mitigation is determined using results from free-field triggering analyses, not because the performance of the mitigation is necessarily tied to triggering in the free-field.

In this study, we first propose probabilistic models for the cumulative absolute velocity required to trigger liquefaction (CAVc), based on data from a comprehensive 1D numerical site response parametric analysis (detailed by Bullock 2020 and Bullock et al. 2022), here referred to as the first parametric study (PS-I). The numerical models in PS-I were calibrated and validated with element level and centrifuge free-field

experiments. The models consider the influence of layer, profile, ground motion properties, as well as system-level effects caused by low-permeability strata within the soil profile. These models describe the uncertainty in evaluating the probability of liquefaction according to a threshold r_u value (e.g., 1.0 in the traditional definition of liquefaction or 0.9 in that of Olson et al., 2020). The results are compared with observations of liquefaction or no liquefaction in the 2010 Darfield, 2011 Christchurch, and 2016 Valentine's Day earthquakes in Canterbury (Geyin et al. 2021), together with other existing predictive models of triggering.

We subsequently extend the triggering model to predict liquefaction-induced permanent settlement (including volumetric and deviatoric deformations) beneath an unmitigated, mat-founded structure based on the centrifuge-calibrated numerical analyses described by Karimi et al. (2018) and Bullock et al. (2019a): PS-II. The initial functional form developed based on the numerical database was then compared with and adjusted based on a case history database consisting of 50 cases from six earthquakes. The adjustment helped account for sedimentation and ejecta effects that were not effectively captured numerically or experimentally in unmitigated models (see Bullock et al. 2019a for additional details). This model incorporates the influence of the soil profile, the presence and 3D properties of the structure, and cumulative characteristics of the ground motion. The model is improved from Bullock et al. (2019a) through removal of the implicit conditioning on the occurrence of liquefaction by applying the Bullock et al. (2022) triggering model for CAVc.

In the end, we extend the numerical database in PS-III to include ground densification around structures (770, 3D, fully-coupled, FEA through quasi-Monte Carlo sampling of key input parameters), which was also calibrated and validated with related centrifuge models. This database is subsequently used to propose a probabilistic predictive procedure for foundation's permanent settlement on liquefiable soils that are improved with ground densification. The models consider realistic, nonlinear, 3D structures on mat foundations or basement, SSI, interlayering and layer cross interactions, ground densification properties and geometry, and ground motion characteristics. Similar to the settlement models for unmitigated cases, we use nonlinear regression with lasso-type regularization to estimate model coefficients. The reliability of the predicted model is subsequently evaluated by comparing the trends with a limited number of centrifuge and field case histories. With the small number of well-documented case histories available on mitigated buildings, no further model adjustment was possible in this case. However, this was judged acceptable at this time, due to the relatively small error observed in case history predictions.

The proposed set of models are the first of their kind to comprehensively consider the triggering, consequences, and mitigation of soil liquefaction near structures and the underlying uncertainties in a unified and explicit manner, aiming to guide a more reliable and performance-based treatment of liquefiable soils near structures.

2 Case History Collection

The case histories related to each of the three analysis phases (PS-I through PS-III) are summarized in Table 1. In PS-III, the case history database involving ground densification around shallow-founded structures was too small for a meaningful statistical

evaluation and adjustment. Hence, the limited case histories (see Table 1) that included mitigation and some information about the soil and structure were only used to evaluate the performance of the predictions from the proposed settlement model on densified ground. The representative case history was collected during the 1964 Niigata, Japan Earthquake. In Niigata City, liquefaction-induced damage on mitigated ground was documented (Watanabe 1966), including one oil tank and one shallow-founded building. The mitigated site near Hakusan district (Kawakami and Asada 1966) included a 14 m-thick, fine sand layer with a D_r of about 90% (in average), followed by a 10 m-thick, sandy soil with a $D_r \approx 60\%$ ($N_{1,60}$ ranging from 10 to 20). Subsequently, both layers were overlaid by 6 m of a silty sand layer deposit with a $D_r \approx 30\%$ ($N_{1,60}$ ranging from 3 to 6). The liquefiable layer was identified (Ishihara and Koga 1977) from a depth of about 3 m to 13 m below the ground surface, based on the cyclic triaxial tests on undisturbed specimens. For additional details on the case history listed in Table 1, please refer to Hwang et al. (2022b).

Table 1. Source and quantity of case histories related to each parametric study (PS).

PS	Source	Earthquake	No. of cases
I[(a)]	Geyin et al. 2020, 2021	Darfield, 2010	997
		Christchurch, 2011	3846
		Valentine's Day, 2016	155
II[(b)]	Yoshimi and Tokimatsu (1977)	Niigata, 1964	15
	Acacio et al. (2001)	Luzon, 1990	17
	Bray and Sancio (2009)	Kocaeli, 1999	3
	Unutmaz and Cetin (2010)	Kocaeli and Düzce, 1999	27
	Bertalot et al. (2013)	Chile, 2010	21
	Bray et al. (2014)	Christchurch, 2011	4
III[(c)]	Yoshida (2000)	Kobe, 1995	1
	Watanabe (1966)	Niigata, 1964	2

[(a)] Additional details in Bullock et al. (2022)
[(b)] Additional details in Bullock et al. (2019a)
[(c)] Additional details in Hwang et al. (2022)

3 Centrifuge Modeling

Five centrifuge tests were conducted under a centrifugal acceleration of 70g at the University of Colorado Boulder's 5.5 m-radius, 400 g-ton centrifuge facility (Olarte et al. 2017, 2018a; and Paramasivam et al. 2018), to investigate seismic site response in a layered, liquefiable, free-field soil profile (with no structures present) and the influence

of ground densification on shallow-founded, potentially inelastic structures on liquefiable soils. The tests including structures examined two types of moment-resisting frame structures (a 3-story Structure A on a 1 m-thick mat foundation and a heavier, taller, and more flexible, 9-story Structure B on a 1-story basement foundation) and one layered, liquefiable soil profile with and without ground densification, as shown in Figure 1. Structures A_{NM} or B_{NM} in these tests represented Structures A or B on an unmitigated soil profile, while A_{DS} or B_{DS} represented the same structures and soil profile, now including ground densification.

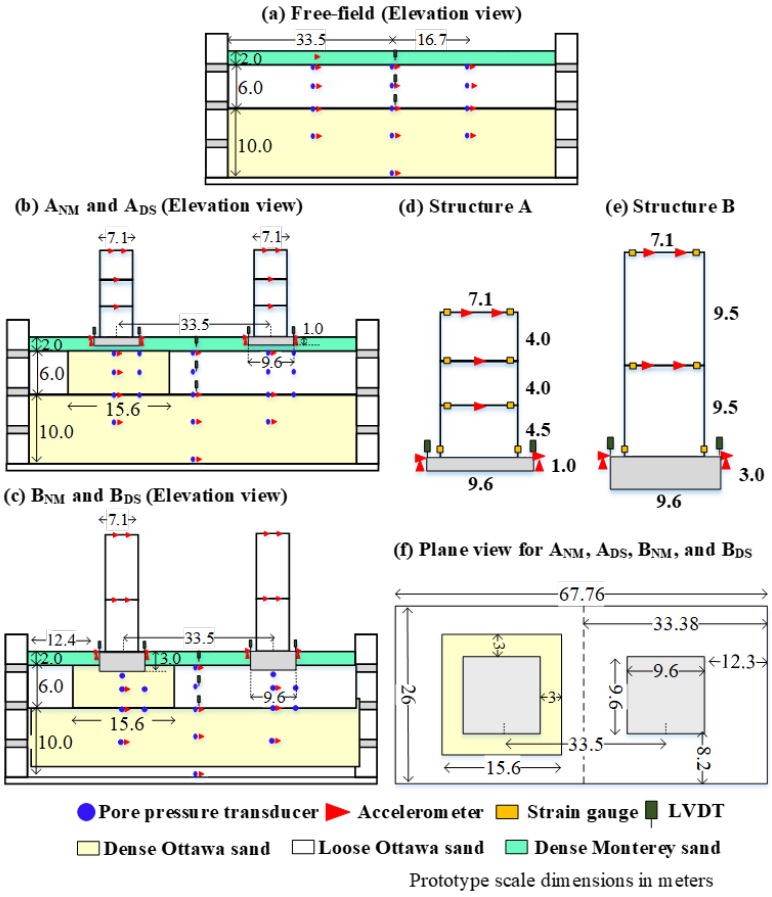

Fig. 1. Configuration and instrumentation layout of the centrifuge experiments used for numerical model validation. (All units are in prototype scale meters at 70g of centrifugal acceleration.)

In all centrifuge tests, a 10 m-thick (in prototype scale) dense Ottawa sand F65 layer was dry-pluviated to attain a relative density (D_r) of approximately 90% (e_{min} = 0.53 and e_{max} = 0.81), prior to testing. Subsequently, a 6 m-thick loose Ottawa sand layer was dry pluviated to reach a D_r of 40%. Above this layer, a 2 m-thick Monterey sand layer was dry pluviated to attain a $D_r \approx 90\%$ (e_{min} = 0.54 and e_{max} = 0.84) as a dense, draining crust. The groundwater table in all centrifuge tests was located at the ground surface. The mitigated (densified) zone was attained by dry pluviating Ottawa sand with

a $D_r \approx 90\%$ around Structures A_{DS} or B_{DS}. The entire thickness of looser Ottawa sand was treated (i.e., 6 m), with the densification width beyond the foundation edges selected as half of the densification depth (i.e., 3 m), based on JGS (1998).

All model specimens were spun to a nominal centrifugal acceleration of 70*g*. A series of four one-dimensional (1D) horizontal earthquake motions was applied to each model after saturation (with a methylcellulose solution 70 times more viscous than water). For numerical validation in the free-field or below the unmitigated or mitigated structure, we only used the first major motion, prior to which the soil properties and geometry were known with greater accuracy. All units presented in this paper are in the prototype scale. The subsequent numerical simulations of these tests were also performed in prototype scale units. Detailed discussions of all centrifuge tests were provided by Olarte et al. (2017, 2018a) and Paramasivam et al. (2018), which are not repeated here for brevity.

4 Numerical Modeling Details

Three-dimensional (3D), fully coupled, FE simulations were performed in the object-oriented, parallel computation FE platform OpenSees (Mazzoni et al. 2006). The pressure-dependent, multi-yield surface, version 2, soil constitutive model (Elgamal et al. 2002 and Yang et al. 2008), PDMY02, was used to simulate the nonlinear response of saturated, granular soils and consequences of liquefaction-induced ground deformations (Karimi et al. 2016a,b; Ramirez 2018; and Hwang et al. 2021).

The PDMY02 model parameters used for Ottawa sand at a handful of relative densities (30%, 40%, 50%, 60%, 70%, 80%, and 90%) were adopted from Hwang et al. (2021). The calibration process was based on: i) a series of fully drained and undrained, monotonic and cyclic triaxial tests (Badanagki 2019); ii) a boundary value problem involving free-field site response as recorded in centrifuge with the same soil types but no structure or mitigation involved (Fig 1a, Ramirez et al. 2018); and iii) empirical observations of liquefaction triggering in terms of number of cycles to liquefaction (NCEER 1997). The best-fitting PDMY02 soil constitutive model parameters were consequently identified by minimizing the sum of root mean squared error (RMSE) among all numerical results and experimental or field observations equally. Figs. 2a-c compare the experimental data (e.g., cyclic triaxial test, free-field site response, and CSR to trigger liquefaction in 15 cycles) and numerically computed response (by adopting the best-fitting parameters) to demonstrate that the calibrated PDMY02 parameters could roughly capture the dynamic behavior of Ottawa sand from an element level to a boundary value problem and to field observations of liquefaction. Additional data and comparisons (e.g., monotonic triaxial tests) are provided by Hwang et al. (2021; 2022a,b).

After calibration, the numerical models of the entire soil-foundation-structure system with and without densification were validated with the corresponding centrifuge experiments (e.g., Figs. 3b-3c). 3D, 20-8 nodes, serendipity, brick elements with the u-p formulation (Zienkiewicz et al. 1990) were used to model the soil domain. The fluid bulk modulus was assumed to be 2×10^6 kPa at atmospheric pressure. The element size was calculated at each depth based on the soil's empirical small-strain shear wave

velocity profile (Seed and Idriss 1970; Bardet et al. 1993; and Menq 2003) and the minimum wavelength of interest (detailed by Ramirez et al. 2018 and Hwang et al. 2021).

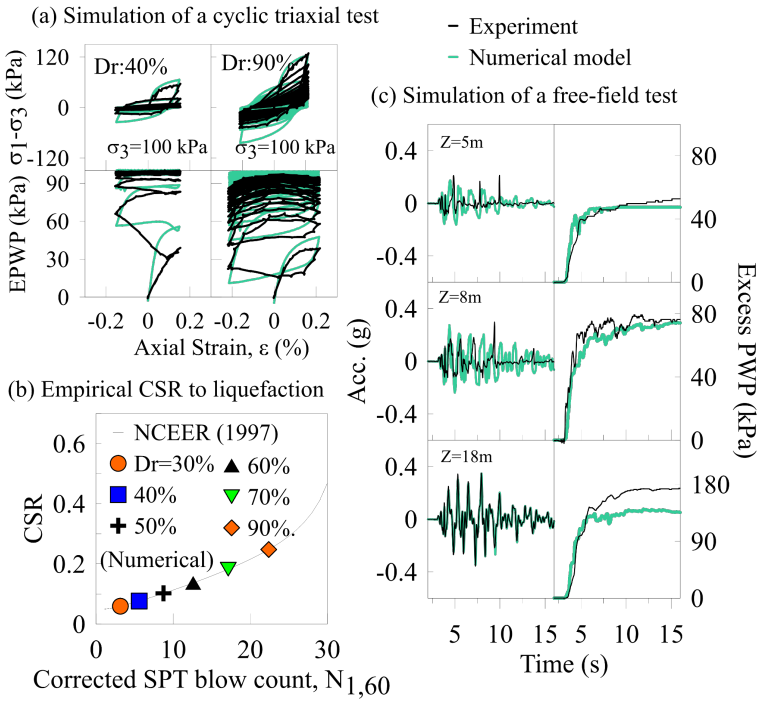

Fig. 2. Calibration of constitutive model (PDMY02) parameters: (a) comparison of numerical simulations with a representative strain-controlled cyclic triaxial experiments on Ottawa Sand (isotropic consolidation stress = 100 kPa; axial strain amplitude = 0.2%); (b) comparison of numerical simulations with empirical observations in terms of CSR to trigger liquefaction in 15 cycles for different relative densities ($N_{1,60}=35D_r^2$; Skeptom 1986); (c) comparison of numerical simulations with a free-field centrifuge experiment using the same soil profile (see Fig. 1a).

The foundations were modeled with 20-8 node brick u-p elements and the linear-elastic material. Note that the fluid mass density was set to zero in the foundation to avoid generation of excess pore pressures. The foundation-soil interface was modelled with an equal degrees-of-freedom (DOF) connection to the soil (Karimi and Dashti 2016a,b and Hwang et al. 2021). To allow for relative settlement of foundation with respect to the surrounding soil, the nodes around the foundation's lateral perimeter were tied to soil only in the horizontal direction (e.g., x- and y-directions).

The beams and columns in Structures A and B were modeled with elastic beam-column elements and a linear-elastic material, while the reduced section "fuses", where structural nonlinearity localized, were modeled with a nonlinear fiber section and the uniaxial steel material. A damping ratio of 0.8% and 1.2% was assigned to Structures A and B, respectively. These properties were calibrated with component tests as well

as fixed-base hammer impact tests. Details of the design and calibration of structure parameters were reported by Olarte (2017) and Ramirez (2019).

In models involving the soil-foundation-structure system, half of the model container (in the direction perpendicular to shaking) was simulated by taking advantage of symmetry (Karimi and Dashti 2016a, b; Ramirez 2019; and Hwang et al. 2021). The lateral boundary nodes located at the same elevation were tied to move together in both horizontal directions, roughly representing the conditions in a flexible-shear-beam container. The bottom boundary of the soil domain was fixed in all translational directions (i.e., x-, y-, and z-directions) when modeling the centrifuge tests, to simulate the rigid container base. The length and width of the soil domain were, however, increased compared to the container, in order to reduce the adverse effects of reflecting waves from the boundaries and displacement constraints near the center of the domain (where the structure was placed). The minimum numerical domain length (parallel to shaking) was, accordingly, determined as 6B (where B is the foundation width) and the domain width (perpendicular to shaking) as 3B through an initial sensitivity study. Note that this same domain size (6B in length and 3B in width) was adopted for the subsequent numerical parametric studies PS-I through III. The excess pore pressures were only allowed to dissipate through the domain surface. The acceleration time history recorded at the base of the container in centrifuge during the first major motion was applied directly to the base nodes of the numerical models after reaching static equilibrium.

Comparisons of experimental and numerical results in terms of 5%-damped acceleration response spectra and settlement time history of foundations as well as excess pore pressure-time history and acceleration response spectra in the middle of the critical layer (z = 5 m) are provided in Fig. 3. These results show that overall, numerical simulations of unmitigated and mitigated isolated structures like A and B roughly captured spectral accelerations near the structure's fundamental period, peak excess pore pressures, and foundation's average permanent settlement observed experimentally (difference of less than about 9, 24, and 6% in each response, respectively). However, the numerical models overestimated the dilation cycles (as sharp drops in excess pore pressures or spikes in acceleration) within the looser (unmitigated) Ottawa sand layer, particularly below the lighter Structure A. This was due to an over-estimation of shear strain excursions because of soil softening, encouraging cycles of re-stiffening and acceleration spike at lower periods. Accordingly, accelerations were slightly over-estimated on the foundation and roof of Structure A near its fundamental period ($T_{o\text{-}A} \approx 0.56$ s) and the motion's mean period ($T_m \approx 0.9$ s). The differences were reduced substantially for mitigated (densified) cases with smaller shear strains and pore pressures.

In general, the treated soil below Structures A_{DS} and B_{DS} experienced smaller excess pore water pressures and settlements compared to their unmitigated counterparts, both experimentally and numerically. This is because increasing soil relative density (Dr) increases its stiffness and strength, reducing its contractive tendencies and hence, net generation of excess pore water pressures. A reduction in the degree of soil strength loss reduced the contribution of volumetric and shear deformations below the structure. In general, 3D, fully-coupled, effective-stress, finite element models with a well-calibrated constitutive model and numerical setup (e.g., with use of higher order elements and sufficient boundary size) could capture the primary experimental patterns. Considering all sources of error and uncertainty in both experimental and numerical models,

we judged the comparisons to be reasonable, particularly for mitigated or densified conditions, and moved on with the design of three parametric studies.

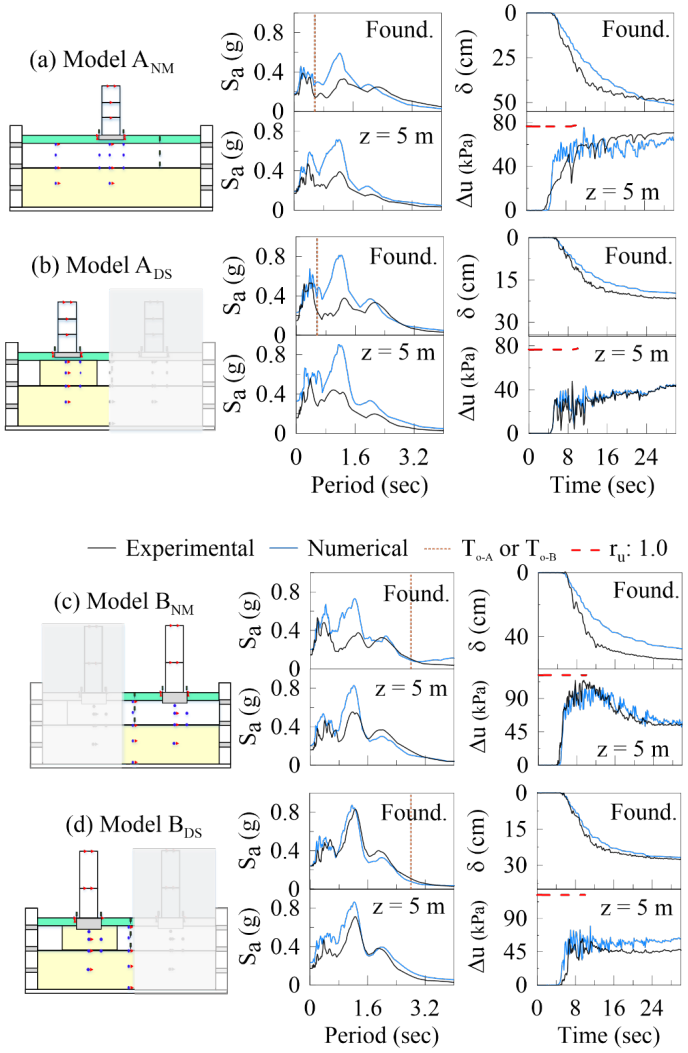

Fig. 3. Comparison of experimental and numerical results in terms of 5%-damped acceleration response spectra and settlement time histories of foundations as well as excess pore pressure-time histories and acceleration response spectra under the center of isolated structures in the middle of the critical layer (z = 5 m) during the Kobe-L motion recorded in the centrifuge.

5 Numerical Parametric Studies

The schematic view of typical 3D models used in the numerical parametric studies PS-I through III are shown in Fig. 4. The numerical framework, selection of elements, and loading conditions were consistent with the results and conclusions presented in the previous section. However, in the parametric studies, our goal was also to account for variations in structural type and properties, soil layering, rock's elastic properties, and ground motion characteristics.

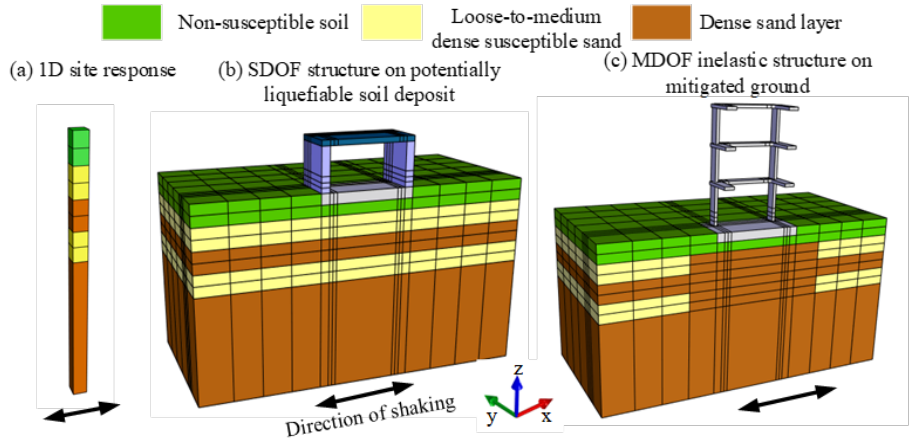

Fig. 4. Schematic drawings showing the numerical simulation of: (a) a 1D single soil column for nonlinear site response analyses in PS-I; (b) a SDOF, isolated, elastic structure on a layered liquefiable deposit in PS-II; and (c) an MDOF, isolated, potentially inelastic structure on a layered liquefiable deposit improved with ground densification in PS-III.

For developing the liquefaction triggering models in the free-field, the simulations in PS-I focused on free-field conditions (using single-column, 1D, nonlinear site response analyses). The PS-II for the consequence model without mitigation involved 3D, linear-elastic, single-degree-of-freedom (SDOF) structures on mat foundations. A linear and elastic structural response was judged reasonable given the large degree of nonlinearity and damping in the underlying unmitigated soil. In contrast, the PS-III for ground improvement focused on inelastic (damageable), multi-degree-of-freedom (MDOF) structures representative of the building stock in seismically active regions of the U.S. founded on mat foundations and layered, liquefiable, soil profiles treated with ground densification. The considered soil profiles included liquefiable, loose- to medium-dense, saturated, clean sand layers as well as dense sand interlayers and in some models, a thin silt capping layer. Ground densification was only applied to portions of the most critical, loose to medium dense granular layer(s) in the parametric study.

To ensure all input parameters (IPs) characterizing the soil-foundation-structure system and when applicable, the mitigation geometry, were adequately and uniformly represented in the parameter space, a quasi-Monte Carlo sampling procedure was adopted to select the initial model suites in each PS (see Table 2). Each IP was initially drawn

from either a uniform or a triangular distribution. These ranges and distributions were informed by a combination of: (1) observed values of these parameters in the Bullock et al. (2019a) case history database of buildings on liquefiable soils; and (2) ranges considered and shown as influential in the numerical database previously generated by Karimi et al. (2018). Subsequently, the corresponding parameter combinations were determined by taking the inverse cumulative distribution functions from a quasi-random set of numbers between 0 and 1 for each IP. In total, in PS-III a suite of 70 basic model configurations was designed by quasi-Monte Carlo sampling to account for variations in soil-foundation-structure systems and mitigation design. PS-II included a suite of 420 model configurations designed to facilitate sensitivity analysis for each independently-varied parameter. PS-I included 125 model configurations, determined using quasi-Monte Carlo sampling, which were each analyzed using three soil constitutive models to facilitate quantification of epistemic uncertainty. For additional details on the parameter distributions for soil layer, structural, rock, densification, and ground motion properties in each of the three PS's, please refer to Bullock et al. (2019a), Bullock et al. (2022), and Hwang et al. (2022b).

Table 2. The main input parameters (IPs) in the numerical parametric study (PS) I, II, and III.

Parametric study ID	The main IPs in the numerical parametric study
PS-I	· Number, thickness, and density of the loose to medium-dense sand layers. · Total deposit thickness above bedrock. · Bedrock shear wave velocity. · Presence of low-permeability strata throughout the profile. · Ground motion intensity measures.
PS-II	· The same main IPs as PS-I. · Foundation bearing pressure, footprint size, and embedment depth. · Height and inertial mass of elastic structure.
PS-III	· The same main IPs as PS-I and PS-II. · Nonlinear structural properties including wood-frame, reinforced concrete moment frame, and steel moment frame buildings. · Ground densification design in terms of depth and width beyond the foundation edge.

6 Statistical Modeling and Initial Functional Forms

The Bullock et al. (2019a) settlement model consists of a base model developed using a database of 63,000 numerical analyses of soil-foundation-structure systems (PS-II) and adjusted according to a database of 50 empirical case histories. The base model captures the relationships among soil, foundation, and structure-specific parameters and

settlement, as well as the ground motion intensity and its interaction with other parameters. The functional form of the base model is given by:

$$ln(\delta) = f_{soil} + f_{fnd} + f_{str} \quad \text{Eq. 1}$$

where $ln(\delta)$ is the natural logarithm of the median predicted foundation settlement (in units of mm) and f_{soil}, f_{fnd}, and f_{str} are functions that reflect how a shallow-founded structure's settlement is influenced by properties of the soil, foundation, and structure, respectively.

Equations 2 - 6 describe f_{soil}, where $H(\cdot)$ is the Heaviside step function of the argument, $H_{S,i}$ is the thickness of the i-th liquefaction-susceptible layer (in units of m), ε is an infinitesimal positive quantity, CAV is the outcropping rock cumulative absolute velocity (in units of cm/s), $q_{c1N,i}$ is the normalized CPT cone tip resistance of the i-th liquefaction-susceptible layer, $D_{S,i}$ is the depth from the foundation to the center of the i-th liquefaction-susceptible layer (in units of m), and F_{LPC} is a flag that is equal to 1 if there is a low-permeability cap at the top of the soil profile and 0 otherwise.

$$f_{soil} = [\Sigma_i H(H_{S,i} - 1 + \varepsilon) f_{S,i} f_{H,i}] + [c_0 + c_1 ln(CAV)] F_{LPC} + s_0 ln(CAV) \quad \text{Eq. 2}$$
$$f_{S,i} = a_0 \text{ for } q_{c1N,i} < 112.4 \quad \text{Eq. 3}$$
$$f_{S,i} = a_0 + a_1(q_{c1N,i} - 112.4) \text{ for } 112.4 \leq q_{c1N,i} < 140.2 \quad \text{Eq. 4}$$
$$f_{S,i} = a_0 + 27.8a_1 \text{ for } 140.2 \leq q_{c1N,i} \quad \text{Eq. 5}$$
$$f_{H,i} = b_0 H_{S,i} exp[b_1(max(D_{S,i}, 2)^2 - 4)] \quad \text{Eq. 6}$$

Equations 7-9 describe f_{fnd}, where q is the foundation bearing pressure (in units of kPa), $D_{S,1}$ is the depth from the foundation to the center of the top-most liquefaction-susceptible layer in the soil profile (in units of m), B is the foundation width (in units of m), L is the foundation length (in units of m), and D_f is the foundation embedment depth (in units of m). The foundation width (B) is defined as its shorter dimension (i.e., $L/B \geq 1$).

$$f_{fnd} = f_q + f_{B,L} \quad \text{Eq. 7}$$
$$f_q = \{d_0 + d_1 ln[min(CAV, 1000)]\} ln(q) \times exp\{d_2 min[0, B - max(D_{S,1}, 2)] \quad \text{Eq. 8}$$
$$f_{B,L} = \{e_0 + e_1 ln[max(CAV, 1500)]\} ln(B)^2 + e_2 L/B + e_3 D_f \quad \text{Eq. 9}$$

Equation 10 describes f_{str}, where h_{eff} is the structure's effective height (in units of m) and M_{st} is the structure's inertial mass (in units of kg).

$$f_{str} = \{f_0 + f_1 ln[min(CAV, 1000)]\} {h_{eff}}^2 + f_2 min[M_{st}/10^6, 1] \quad \text{Eq. 10}$$

Equation 11 describes the adjustment to the base model's prediction of settlement, where $ln(\delta_{adj})$ is the adjusted prediction of settlement (in units of mm) and $H_{S,1}$ is the thickness of the top-most liquefaction-susceptible layer (in units of m). In the case history database, $H_{S,1}$ is usually also the thickest liquefaction-susceptible layer, and we may therefore consider $H_{S,1}$ to be the thickness of the "critical" layer, which can be identified as the layer with the highest value of $f_{S,i} f_{H,i}$ as described above. This approach treats the critical layer as the one contributing the most to settlement.

$$ln(\delta_{adj}) = ln(\delta) + k_0 + k_1 min(H_{S,1}, 12)^2 + k_2 min(q, q_c) + k_3 max(q - q_c, 0) \geq ln(\delta) \quad \text{Eq. 11}$$

Bullock et al. (2019a) also provided the logarithmic standard deviation of a lognormal distribution around δ_{adj}, denoted as σ_{adj}. Table 3 provides the model coefficients for Bullock et al. (2019a):

Table 3. Model coefficients for Bullock et al. (2019a)

Parameters	Value	Parameters	Value
a_0	1.000	e_3	-0.2148
a_1	-0.0360	f_0	-0.0137
b_0	0.3026	f_1	0.0021
b_1	-0.0205	f_2	0.1703
c_0	1.3558	s_0	0.4973
c_1	-0.1340	k_0	-1.5440
d_0	-1.3446	k_1	0.0250
d_1	0.2303	k_2	0.0295
d_2	0.4189	k_3	-0.0218
e_0	-0.8727	q_c	61
e_1	0.1137	σ_{adj}	0.6746
e_2	-0.0947		

The lognormal distribution defined by δ_{adj} and σ_{adj} can be used to formulate the probability of exceeding settlement thresholds of interest (i.e., those related to certain repair actions). Here, we denote a threshold value of settlement as δ_{thresh}. However, note that these probabilities are implicitly conditioned on the occurrence of liquefaction due to the correction based on case history observations that included observations of liquefaction surface manifestation. Equation 12 shows the calculations needed to obtain a conditional probability of exceedance based on the Bullock et al. (2019a) model, where Liq is a flag that indicates the triggering of liquefaction and $\Phi[\cdot]$ is the standard normal cumulative distribution function evaluated at the argument.

$$P(\delta_{adj} > \delta_{thresh}|Liq) = 1 - \Phi[(ln(\delta_{thresh}) - ln(\delta_{adj}))/\sigma_{adj}] \quad \text{Eq. 12}$$

As discussed above, this conditioning arises because (i) the case history adjustment is based only on cases where liquefaction damage was observed; and (ii) the numerical database was filtered to include only observations with $\delta \geq 10$ mm. A probabilistic liquefaction triggering model is needed to remove this conditioning.

Bullock et al. (2022) developed liquefaction triggering models in the free-field based on CAV using the results of PS-I. These models give estimates of the capacity cumulative absolute velocity (CAV_c) in units of cm/s. CAV_c is defined as the input outcropping rock CAV needed to generate a certain r_u value in a given soil element. Equation 13 describes CAV_c:

$$ln(CAV_c) = a_0 + a_1\sqrt{z} + a_2[f_{lps}/(z_{lps} + z)] + a_3(q_{c1N}/100) \quad \text{Eq. 13}$$

where $ln(CAV_c)$ is the natural log of the median predicted capacity CAV, z is the depth from the ground surface to the soil element (in units of m), f_{lps} is a flag that indicates

whether there is a low-permeability stratum anywhere above the soil element in the profile, and z_{lps} is the depth from the soil element to the nearest low-permeability stratum above (in units of m). Table 4 provides the model coefficients for Bullock et al. (2022) for CAV_c corresponding to an r_u threshold of 0.9 [i.e., *liquefaction* according to Olson et al. (2020)].

Table 4. Model coefficients for estimating CAV_c in Bullock et al. (2022).

Parameters	Value	Parameters	Value
a_0	4.640	a_3	0.273
a_1	0.167	σ_c	0.675
a_2	-0.877	ρ_{dc}	0.249

CAV_c can be combined with the outcropping rock CAV to obtain a factor of safety against liquefaction triggering (FS_{liq}):

$$FS_{liq} = CAV_c/CAV \quad \text{Eq. 14}$$

$$ln(FS_{liq}) = ln(CAV_c) - ln(CAV) \quad \text{Eq. 15}$$

The Bullock et al. (2022) free-field liquefaction triggering model can also be used to obtain probabilities of liquefaction that are consistent with the functional form and approach used in the consequence model proposed by Bullock et al. (2019a). Equation 15 can be rewritten in terms of variables from Bullock et al. (2019a) to obtain the median FS_{liq} in the center of the critical layer as follows:

$$ln(FS_{liq,l}) = a_0 + a_1\sqrt{D_{S,l} + D_f} + a_2[f_{lps}/(z_{lps} + D_{S,l} + D_f)] + a_3(q_{clN,l}/100) - ln(CAV) \quad \text{Eq. 16}$$

where $ln(FS_{liq,l})$ is the natural logarithm of the median predicted factor of safety in the center of the critical layer and $q_{cln,l}$ is the normalized cone tip resistance in that layer.

Bullock et al. (2022) provides the correlation coefficient between the uncertainties around CAV_c and CAV, denoted as ρ_{dc}. The logarithmic standard deviation of the factor of safety, σ_f, is given by Equation 17, where σ_c is the logarithmic standard deviation around the median CAV_c and σ_d is the logarithmic standard deviation around the median outcropping rock CAV.

$$\sigma_f = \sqrt{\sigma_c{}^2 + \sigma_d{}^2 + 2\rho_{dc}\sigma_c\sigma_d} \quad \text{Eq. 17}$$

We can obtain the probability of liquefaction triggering (i.e., the probability of FS_{liq} less than 1.0) using the lognormal distribution:

$$P(Liq) = \Phi[-ln(FS_{liq,l})/\sigma_f] \quad \text{Eq. 18}$$

This equation can be combined with Equation 12 to obtain the marginal probability of settlement exceeding a threshold value (i.e., the probability without conditioning on Liq):

$$P(\delta_{adj} > \delta_{thresh}) = P(\delta_{adj} > \delta_{thresh}|Liq)P(Liq) \quad \text{Eq. 19}$$

Following the development of triggering and consequence models described above, a total of 770 numerical simulations using three-dimensional (3D), fully-coupled, non-linear finite element analyses of the soil-foundation-structure systems enabled a comprehensive evaluation of the seismic performance of shallow-founded structures on treated soils. The detailed properties of all numerical analyses are provided in Hwang et al. (2022). The nonlinear regression with lasso-type (Tibshirani 1996) regularization was used to develop the predictive model for permanent settlement of structures on densified soils.

Equation 20 shows the general functional form for estimating permanent settlement of structures on liquefiable deposit improved by ground densification:

$$ln\ ln\ (\delta_{DS}) = \alpha_0 + f_{FN-ST} + f_{SL-DS} + f_{UD} + f_{GM} \quad \text{Eq. 20}$$

where $ln\ ln\ (\delta_{DS})$ is the natural logarithm of the median predicted foundation settlement (in units of mm) on densified soils, α_0 is a constant intercept. f_{FN-ST}, f_{SL-DS}, f_{UD}, and f_{GM} are functions that reflect how structure's settlement is influenced by the foundation (FN)-structure (ST) system, layered soil profile (SL) and densification properties (DS), the properties of any remaining undensified loose- to medium-dense soil layer (UD) below the densified zone within foundation's influence zone, and an optimum ground motion intensity measure (GM). The functional forms for f_{FN-ST}, f_{SL-DS}, f_{UD}, and f_{GM} are described by Equations 21-25.

$$f_{FN-ST} = \alpha_1 D_f + ln\ \alpha_2 ln\ (B) + ln\ \alpha_3 ln\ (q) + ln\ \alpha_4 ln\ \left(\frac{H}{B}\right) + \alpha_5\ ln\ ln\ \left(\frac{L}{B}\right) \quad \text{Eq. 21}$$

$$f_{SL-DS} = ln\ \alpha_6 ln\ \left(H_{dep}\right) + + \alpha_8 ln\ \left(\frac{D_{DS}}{H_L}\right) + \alpha_9 D_{r,DS} \quad \text{Eq. 22}$$

$$f_{UD} = \alpha_{10} f_{D_r(H_{UD})} + \alpha_{11} H_{UD} \quad \text{Eq. 23}$$

$$f_{D_r(H_{UD})} = \begin{cases} 0, & H_{UD} = 0 \\ D_r\ of\ undensified\ layer, & H_{UD} > 0 \end{cases} \quad \text{Eq. 24}$$

$$f_{GM} = \begin{cases} \alpha_{12}\ ln\ ln\ (CAV) & , CAV < 450 cm/s \\ \alpha_{12} ln\ (450) + \alpha_{13}\ ln\ ln\ \left(\frac{CAV}{450}\right) & , CAV \geq 450 cm/s \end{cases} \quad \text{Eq. 25}$$

where D_f is the foundation embedment depth from the ground surface (in m), B is the foundation width (in m), q is the bearing pressure of the foundation-structure system (in kPa), H/B is the unitless actual structure height to width ratio, L/B is the unitless mat foundation length (L) to width (B) aspect ratio, H_{dep} is the total deposit depth above bedrock (in m), H_L is the total cumulative thickness of critical, loose- to medium-dense granular soil layers (i.e., the summation of layer thickness with $D_r \leq 70\%$ within foundation's influence zone (defined as 1.5B in this model) in m, W_{DS} is the densification width beyond the edges of the foundation (in m), D_{DS} is the densification depth from ground surface (in m), $D_{r,DS}$ (in percentage) is the target relative density of the treated soil, where $f_{D_r(H_{UD})}$ is a flag that is equal to the average relative density (%) of the undensified layer if the densification depth does not reach the full depth of the deepest critical layer within the foundation's influence zone; or is zero otherwise. H_{UD} is the thickness of the remaining undensified, loose- to medium-dense granular soil layer

within the foundation's influence zone (in m). CAV is calculated on outcropping bedrock (in cm/s), while the threshold value of CAV was determined as 450 cm/s through nonlinear regression. All regression coefficients, $\alpha_0 - \alpha_{13}$, are listed in Table 5. The predictive model (Equation 21) can be characterized with a lognormal distribution by passing the Lilliefors (1967) test at the 5% significance level. This indicates that the uncertainty in foundation residual settlement on densified sites could be characterized with a lognormal distribution and a standard deviation (σ) of 0.54.

Table 5. Model coefficients for predicting foundation settlement on mitigated ground.

Parameters	Value	Parameters	Value
α_0	-4.49	α_8	-0.1556
α_1	-0.1998	α_9	-0.001
α_2	-0.3333	α_{10}	-0.0047
α_3	0.8604	α_{11}	0.0861
α_4	-0.1169	α_{12}	0.4766
α_5	0.2632	α_{13}	1.386
α_6	0.6577	σ_{DS}	0.54
α_7	-0.0711		

7 Predictive Model Validation with Case Histories

The Bullock et al. (2019a) settlement models were validated and adjusted with case history data. The case history adjustment described above used a database of 50 case histories of structures on mat foundations that were affected by liquefaction-induced settlement. The adjusted model was then used to predict the settlement of 37 additional shallow-founded structures with other foundation types that were treated as equivalent mat foundations (i.e., mat foundations with dimensions equal to the building footprint). The model's predictions for those cases, which were excluded from the development of the adjustment, were unbiased and their residuals pass a two sample Kolmogorov-Smirnov test in comparison to the lognormal distribution obtained while regressing the adjustment.

The Bullock et al. (2022) models were developed using only data from the PS-I numerical study, with no case history adjustments. As discussed above, the soil models used in this study were calibrated and validated using element-level laboratory tests, centrifuge tests, and field observations. The models for CAV_c themselves were used to develop an LPI-style manifestation model that was shown to perform similarly to existing models for predicting observations of free-field surface liquefaction manifestations.

Fig. 5 shows the exceedance probability curve of foundation settlement for the oil tank and building on densified ground in Niigata city, Japan, during the 1964 Niigata earthquake. These results compared well with the range of observed settlements in the field with an average difference of about 6.3%. The model validation with the very limited case history observations may suggest that our probabilistic model roughly captures the settlement patterns expected in realistic soil profiles. In PS-III, the contribution

of sedimentation and ejecta (mechanisms not well captured numerically) were expected to be less significant than unmitigated conditions. For example, Hausler (2002) showed 18 case histories related to ground densification with various qualities/extents of densification, with little to no evidence of ground failure or major damage during previous earthquakes (but no details were reported). However, we acknowledge that further adjustment (similar to the approach in PS-II) should be performed when more well-documented case histories of mitigated structures become available in the future. More detailed model limitations were discussed in Hwang et al. (2022b), which are not repeated here for brevity.

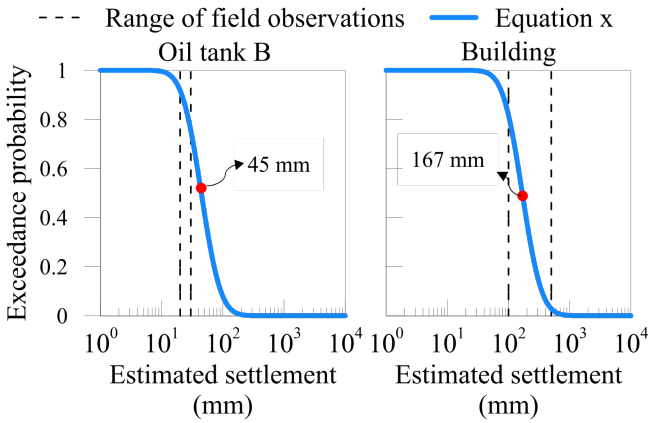

Fig. 5. Exceedance probability curves of structural settlement based on the Niigata City case history example.

8 Concluding Remarks

In this paper, we introduce a comprehensive, unified, and performance-based framework for predicting triggering of soil liquefaction in interlayered deposits, its consequences in terms of seismic settlement near shallow-founded structures, and its mitigation using ground densification. Effective liquefaction mitigation requires an improved fundamental understanding of triggering as a function of excess pore pressures in realistically stratified deposits that experience cross-layer interactions. It also requires improved probabilistic consequence procedures that account for 3D soil-structure interaction (SSI), all mechanisms of deformation, total uncertainty, and the impact of mitigation.

First, a series of centrifuge experiments were performed to evaluate site response and pore pressure generation in layered liquefiable deposits, the dominant mechanisms of deformation in the free-field and near shallow-founded structures, SSI, and the impact of ground densification as a mitigation strategy on SSI. Second, experimental results were used to validate 1D and 3D, fully-coupled, nonlinear, dynamic finite element analyses of layered sites and soil-foundation-structure systems with and without ground densification in OpenSees. Third, three sets of numerical parametric studies (PS-I through PS-III) were used to identify the functional forms for predicting: (i)

liquefaction triggering in the free-field based on the capacity cumulative absolute velocity (CAV_c) corresponding to a threshold excess pore pressure ratio (r_u); (ii) settlement of unmitigated shallow-founded structures on potentially liquefiable soils; and (iii) the relative beneficial impact of ground densification with varying dimensions on foundation's permanent average settlement. In the end, a limited case history database helped validate the triggering and consequence models, accounting for field complexities that are not captured numerically or experimentally. The proposed set of models are the first of their kind to comprehensively consider the triggering, consequences, and mitigation of soil liquefaction near structures and the underlying uncertainties in a unified and explicit manner, aiming to guide a more reliable and performance-based treatment of liquefiable soils near structures.

9 Acknowledgements

The authors acknowledge support from the US National Science Foundation (NSF) under Grant no. 1454431. Any opinions, findings, and conclusions or recommendations expressed in this material are those of the author(s) and do not necessarily reflect the views of the NSF. This work utilized the Summit supercomputer, which is supported by the National Science Foundation (awards ACI-1532235 and ACI-1532236), the University of Colorado Boulder, and Colorado State University.

10 References

[1] Acacio, A.A., Kobayashi, Y., Towhata, I., Bautista, R.T. and Ishihara, K., 2001. Subsidence of building foundation resting upon liquefied subsoil: case studies and assessment. *Soils and Foundations*, *41*(6), pp.111-128.

[2] Bardet, J. P., Q. Huang, and S. W. Chi. 1993. "Numerical prediction for model no 1." In Proc., Int. Conf. on the Verification of Numerical Procedures for the Analysis of Soil Liquefaction Problems, edited by K. Arulanandan and R. F. Scott, 67–86. Rotterdam, Netherlands: A.A. Balkema.

[3] Bertalot, D., Brennan, A.J. and Villalobos, F.A., 2013. Influence of bearing pressure on liquefaction-induced settlement of shallow foundations. *Géotechnique*, *63*(5), pp.391-399.

[4] Bray, J.D. and Sancio, R.B., 2006. Assessment of the liquefaction susceptibility of fine-grained soils. *Journal of geotechnical and geoenvironmental engineering*, *132*(9), pp.1165-1177.

[5] Bray, J., Cubrinovski, M., Zupan, J. and Taylor, M., 2014. Liquefaction effects on buildings in the central business district of Christchurch. *Earthquake Spectra*, *30*(1), pp.85-109.

[6] Boulanger, R. W., and I. M. Idriss. 2012. "Probabilistic standard penetration test–based liquefaction–triggering procedure." J. Geotech. Geoenviron. Eng. 138 (10): 1185–1195. https://doi.org/10.1061/(ASCE)GT .1943-5606.0000700.

[7] Beyzaei, C.Z., Bray, J.D., Cubrinovski, M., Riemer, M. and Stringer, M., 2018. Laboratory-based characterization of shallow silty soils in southwest Christchurch. *Soil Dynamics and Earthquake Engineering*, *110*, pp.93-109.

[8] Bray, J. D., and J. Macedo. 2017. “6th Ishihara lecture: Simplified procedure for estimating liquefaction-induced building settlement.” Soil Dyn. Earthquake Eng. 102 (Nov): 215–231. https://doi.org/10.1016/j .soildyn.2017.08.026.

[9] Bullock, Z., S. Dashti, Z. Karimi, A. Liel, K. Porter, and K. Franke. 2019a. “Probabilistic models for residual and peak transient tilt of mat-founded structures on liquefiable soils.” J. Geotech. Geoenviron. Eng. 145 (2): 04018108. https://doi.org/10.1061/(ASCE)GT.1943-5606.0002002.

[10] Bullock, Z., Z. Karimi, S. Dashti, K. Porter, A. B. Liel, and K. W. Franke. 2019b. “A physics-informed semi-empirical probabilistic model for the settlement of shallow-founded structures on liquefiable ground.” Géotechnique 69 (5): 406–419. https://doi.org/10.1680/jgeot.17.P.174.

[11] Bullock, Z. 2020. “A framework for performance-based evaluation of liquefaction effects on buildings.” Ph.D. dissertation, Dept. of Civil, Environmental, and Architectural Engineering, Univ. of Colorado at Boulder.

[12] Bullock, Z., Dashti, S., Liel, A.B., Porter, K.A. and Maurer, B.W., 2022. Probabilistic Liquefaction Triggering and Manifestation Models Based on Cumulative Absolute Velocity. *Journal of Geotechnical and Geoenvironmental Engineering*, *148*(3), p.04021196.

[13] Badanagki, M. 2019. “Influence of dense granular columns on the seismic performance of level and gently sloped liquefiable sites.” Ph.D. dissertation, Dept. of Civil, Environmental and Architectural Engineering, Univ. of Colorado Boulder.

[14] Cetin, K.O. and Seed, R.B., 2004. Nonlinear shear mass participation factor (rd) for cyclic shear stress ratio evaluation. *Soil Dynamics and Earthquake Engineering*, *24*(2), pp.103-113.

[15] Elgamal, A., Z. Yang, and E. Parra. 2002. “Computational modeling of cyclic mobility and post-liquefaction site response.” Soil Dyn. Earthquake Eng. 22 (4): 259–271. https://doi.org/10.1016/S0267-7261(02)00022-2.

[16] Geyin, M., B. Maurer, B. A. Bradley, R. Green, and S. van Ballegooy. 2020. “CPT-based liquefaction case histories resulting from the 2010–2016 Canterbury, New Zealand, earthquakes: A curated digital dataset (version 2).” DesignSafe-CI. https://doi.org/10.17603/ds2-tygh -ht91.

[17] Geyin, M., B. W. Maurer, B. A. Bradley, R. A. Green, and S. van Ballegooy. 2021. “CPT-based liquefaction case histories compiled from three earthquakes in Canterbury, New Zealand.” Earthquake Spectra 8755293021996367. https://doi.org/10.1177/8755293021996367.

[18] Hwang, Y.W., Ramirez, J., Dashti, S., Kirkwood, P., Liel, A., Camata, G. and Petracca, M., 2021. Seismic interaction of adjacent structures on liquefiable soils: insight from centrifuge and numerical modeling. Journal of Geotechnical and Geoenvironmental Engineering, 147(8), p.04021063.

[19] Hwang, Y.W., Dashti, S. and Kirkwood, P., 2022a. Impact of Ground Densification on the Response of Urban Liquefiable Sites and Structures. *Journal of Geotechnical and Geoenvironmental Engineering*, *148*(1), p.04021175.

[20] Hwang, Y.W., Bullock, Z., Dashti, S., and Liel, A., 2022b. A probabilistic predictive model for the settlement of shallow-founded structure on liquefiable soils improved with ground densification. *ASCE J. Geotech. Geoenviron. Eng*. (accepted and in press).

[21] Idriss, I. M., and R. W. Boulanger. 2008. Soil liquefaction during earthquakes. Berkeley, CA: Earthquake Engineering Research Institute.

[22] JGS, Japanese Geotechnical Society. 1998. "Remedial measures against soil liquefaction." Rotterdam: A.A. Balkema.

[23] Karimi, Z., and S. Dashti. 2016a. "Numerical and centrifuge modeling of seismic soil-foundation-structure interaction on liquefiable ground." J. Geotech. Geoenviron. Eng. 142 (1): 04015061. https://doi.org/10.1061/(ASCE)GT.1943-5606.0001346.

[24] Karimi, Z., and S. Dashti. 2016b. "Seismic performance of shallow founded structures on liquefiable ground: Validation of numerical simulations using centrifuge experiments." J. Geotech. Geoenviron. Eng. 142 (6):04016011. https://doi.org/10.1061/(ASCE)GT.1943-5606.0001479.

[25] Karimi, Z., Dashti, S., Bullock, Z., Porter, K. and Liel, A., 2018. Key predictors of structure settlement on liquefiable ground: a numerical parametric study. *Soil Dynamics and Earthquake Engineering*, *113*, pp.286-308.

[26] Maurer, B. W., S. van Ballegooy, and B. A. Bradley. 2017. "Fragility functions for performance-based ground failure due to soil liquefaction." In Proc., PBD-III: Performance Based Design in Geotechnical Engineering III. Vancouver, BC: International Society for Soil Mechanics and Geotechnical Engineering.

[27] Menq, F. Y. 2003. "Dynamic properties of sandy and gravelly soils." Ph.D. dissertation, Dept. of Civil, Architectural and Environmental Engineering, Univ. of Texas at Austin.

[28] Mazzoni, S., F. McKenna, M. Scott, and G. Fenves. 2006. "Open system for earthquake engineering simulation user command-language." Berkeley, CA: Network for Earthquake Engineering Simulations.

[29] NCEER. 1997. "Proceedings of the NCEER worskhop on evaluation of liquefaction resistance of soils. Technical Report NCEER-97-0022.". National Center for Earthquake Engineering Research.

[30] Olarte, J., B. Paramasivam, S. Dashti, A. Liel, and J. Zannin. 2017. "Centrifuge modeling of mitigation-soil-foundation-structure interaction on liquefiable ground." Soil Dyn. Earthquake Eng. 97: 304–323. https://doi.org/10.1016/j.soildyn.2017.03.014.

[31] Olarte, J., S. Dashti, and A. Liel. 2018a. "Can ground densification improve seismic performance of the soil-foundation-structure system on liquefiable soils." Earth. Eng. Struct. Dyn. : 1–19. https://doi: 10.1002/eqe.3012.

[32] Paramasivam, B., S. Dashti, A. Liel. 2018. "Influence of prefabricated vertical drains on the seismic performance of structures founded on liquefiable soils". J. Geotech. Geoenvirom. Eng. 144(10):04018070. https://ascelibrary.org/doi/abs/10.1061/(ASCE) GT.1943-5606.0001950

[33] Ramirez, J., A. R. Barrero, L. Chen, A. Ghofrani, S. Dashti, M. Taiebat, and P. Arduino. 2018. "Site response in a layered liquefiable deposit: Evaluation of different numerical tools and methodologies with centrifuge experimental results." J. Geotech. Geoenvirom. Eng. 144(10):04018070. https://doi.org/10.1061/(ASCE)GT.1943-5606.0001947.

[34] Ramirez, J. 2019. "Numerical modeling of the influence of different liquefaction remediation strategies on the performance of potentially inelastic structures." Ph.D. dissertation, Dept. of Civil, Environmental and Architectural Engineering, Univ. of Colorado Boulder.

[35] Seed, H. B., and I. M. Idriss. 1970. “Soil moduli and damping factors for dynamic response analyses.” Technical Rep. No. EERRC-70-10, Berkeley, CA: Univ. of California.

[36] Seed, R.B., Cetin, K.O., Moss, R.E., Kammerer, A.M., Wu, J., Pestana, J.M., Riemer, M.F., Sancio, R.B., Bray, J.D., Kayen, R.E. and Faris, A., 2003. Recent advances in soil liquefaction engineering: a unified and consistent framework. In *Proceedings of the 26th Annual ASCE Los Angeles Geotechnical Spring Seminar: Long Beach, CA*.

[37] Olson, S. M., X. Mei, and Y. M. Hashash. 2020. “Nonlinear site response analysis with pore-water pressure generation for liquefaction triggering evaluation.” J. Geotech. Geoenviron. Eng. 146 (2): 04019128. https:// doi.org/10.1061/(ASCE)GT.1943-5606.0002191.

[38] Unutmaz, B. and Cetin, K., 2010. Seismic performance of mat foundations on potentially liquefiable soils after 1999 Turkey earthquakes. *Technical Report METU/GTENG 10/09-02*.

[39] Watanabe, T. 1966. “Damage to oil refinery plants and a building on compacted ground by the Niigata earthquake and their restoration.” *Soils and foundations*, *6*(2), 86-99.

[40] Yang, Z., J. Lu, and A. Elgamal. 2008. OpenSees soil models and solid fluid fully coupled elements: User’s manual. San Diego: Dept. of Structural Engineering, Univ. of California.

[41] Yoshida, N. 2000, January. “Liquefaction of improved ground in Port Island and its effect on vertical array record.” In *Proc. of 12th WCEE* (Vol. 1509).

[42] Yoshimi, Y. and Tokimatsu, K., 1977. Settlement of buildings on saturated sand during earthquakes. *Soils and Foundations*, *17*(1), pp.23-38.

[43] Zienkiewicz, O. C., A. H. Chan, M. Pastor, D. K. Paul, and T. Shiomi. 1990. “Static and dynamic behaviour of soils: a rational approach to quantitative solutions. I. Fully saturated problems.” Proceedings of the Royal Society of London. A. Mathematical and Physical Sciences, 429(1877), 285-309.